JCTC Journal of Chemical Theory and Computation

Article

pubs.acs.org/JCTC

Efficient Implementation of Local Excitation Approximation for Treating Excited States of Molecules in Condensed Phase

Chenyang Zhang, Dandan Yuan, Yang Guo, and Shuhua Li*

School of Chemistry and Chemical Engineering, Key Laboratory of Mesoscopic Chemistry of Ministry of Education, Institute of Theoretical and Computational Chemistry, Nanjing University, Nanjing 210093, P. R. China

ABSTRACT: An efficient implementation of the local excitation approximation (LEA) of time-dependent density functional theory (TDDFT) or time-dependent Hartree−Fock, (TDHF) (or configuration interaction singles, CIS) method has been developed in this work. The LEA-TDDFT, -TDHF, and -CIS methods have been applied to investigate the solvatochromic shift of the $n \rightarrow \pi^*$ vertical excitation energy of acetone in aqueous solution. The main idea of the LEA scheme is that only local electron excitations within a certain active region (called as chromophore) are treated to obtain the excitation energies for locally excited electronic states. We have proposed an efficient localization procedure to obtain regional localized molecular orbitals (RLMOs) localized on the chromophore subunit. To ensure the accuracy of the TDDFT, TDHF, and CIS schemes for the studied system, we choose one acetone and six nearest-neighboring waters as the active region for each acetone−water cluster. For acetone in aqueous solution, the LEA-TDDFT calculations on 600 acetone−water configurations (generated from molecular dynamics simulation) suggest that the blueshift in the $n \rightarrow \pi^*$ vertical electronic excitation energy is 1621 ± 52 cm^{-1}, which is in good agreement with the available experimental blue shift of 1500−1700 cm^{-1}.

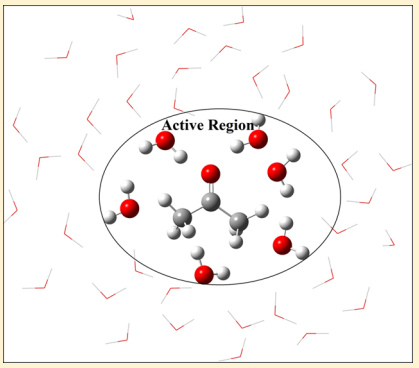

1. INTRODUCTION

Understanding excited electronic states for molecules in condensed phase is very important for many areas in chemistry and material science. A popular way to treat the solvent effect is to adopt a continuum solvent model,[1−3] in which the solvent is modeled as a continuous dielectric of infinite extent that surrounds a cavity containing the solute molecule. For example, polarizable-continuum model (PCM) is one of the dielectric continuum models that can provide satisfactory descriptions on the solvent effect, especially when the solute−solvent interaction is relatively weak.[4−6] However, the cost-effective continuum models are less accurate in describing the effect of highly specific solute−solvent interactions such as hydrogen bonds on electronic absorption spectra.[3,5] Another obvious way of treating molecular excited electronic states in the solvent is to adopt a supermolecule model, which consists of a solute and solvent molecules in the first and second (even third) solvation shells, and perform quantum mechanical calculations for such supermolecules. This approach is able to treat highly specific solute−solvent interactions accurately. However, a major difficulty is that the computational effort of standard excited-state methods increases very steeply with the system size. For small molecules, numerous highly accurate quantum chemical methods for electronic excited states have been established.[7−30] However, these methods are generally inadequate for complex systems in condensed phase, due to the huge computational costs. For medium to large systems, the widely used excited-state methods are the configuration interaction singles (CIS) method,[31] time-dependent Hartree−Fock (TDHF)[32,33] (also known as random phase approximation in physics), and time-dependent density functional theory (TDDFT).[34−36] In fact, these methods still scale as N^4 with N being the number of electrons even if the so-called sigma vectors needed in the Davidson's diagonalization[37] step are directly computed with atomic-orbital two-electron integrals.[31]

However, the computational scaling of the TDDFT, TDHF, or CIS methods can be reduced significantly for those locally excited electronic states, in which the electronic transitions occur in a small active region (called as chromophore) of the whole system. Several theoretical treatments based on local excitation approximations (LEA) have been proposed.[38,39] For instance, Miura et al.[39] developed an efficient LEA scheme to compute locally excited electronic states utilizing the regional localized molecular orbitals (RLMOs) (which are localized at a certain region).[40−43] The basic idea of the LEA scheme is that an approximate TDDFT (or TDHF or CIS) working matrix, in which only singly excited determinants corresponding to local excitations within the chromophore are taken into account, can be used to obtain the excitation energies for locally excited electronic states. Since the dimension of the approximate TDDFT (or TDHF or CIS) working matrix is much smaller than that of the full TDDFT (or TDHF or CIS) working matrix, the computational cost of the LEA-TDDFT (or TDHF or CIS) method is dramatically reduced.

For molecules in the solvent, previous studies showed that a large supermolecule (which contains a solute and many neighboring solvent molecules) is necessary to evaluate their

Received: June 27, 2014

   dx.doi.org/10.1021/ct500551p | J. Chem. Theory Comput. XXXX, XXX, XXX−XXX

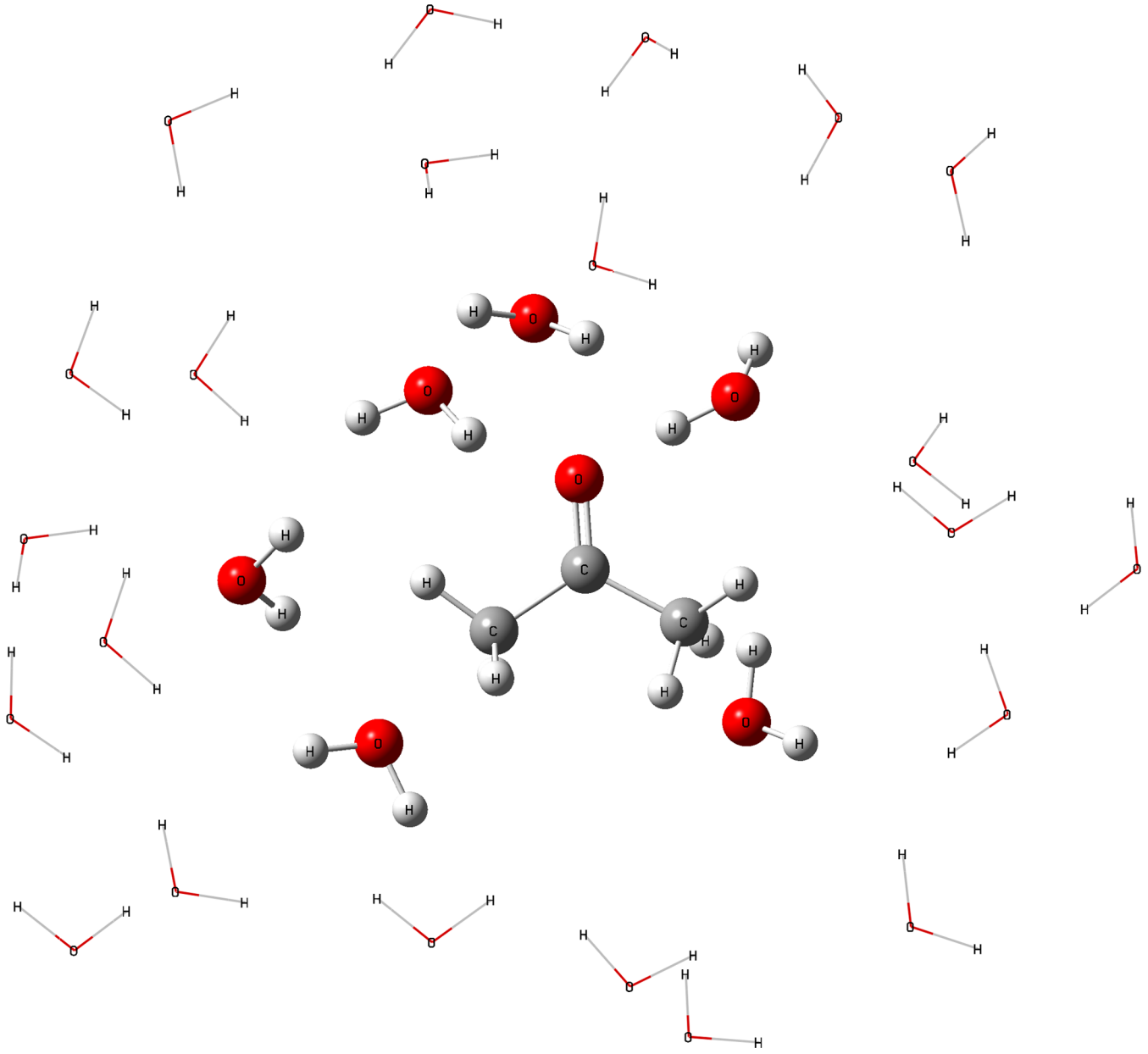

Figure 1. Schematic picture for an acetone−water cluster, in which one acetone and six nearest-neighboring water molecules (denoted by a ball-and-stick model) constitute the active region.

solvatochromic shifts.[44,45] In principle, we could perform direct TDDFT or TDHF (or CIS) calculations for this supermolecule. However, since we need to perform excited state calculations for hundreds of different configurations of such supermolecules (generated from Monte Carlo or Molecular Dynamics simulations) to estimate the solvatochromic shift, this supermolecule approach is computationally quite expensive. In the LEA-TDDFT or TDHF (or CIS) treatment, a small active region, which may contain a solute and a few neighboring solvent molecules, is first chosen, and a subset of regional LMOs are constructed for this active region. Then, the TDDFT or TDHF (or CIS) working matrix corresponding to this active region is solved to obtain the excitation energies. Since the active region is much smaller than the whole supermolecule, the LEA-based supermolecule approach is a computationally affordable approach for treating molecular excited states in the solvent.

The aim of this work is to develop an efficient implementation of the LEA-TDDFT, LEA-TDHF, and LEA-CIS methods for treating molecular excited states in the condensed phase. We propose an efficient method to get the regional localized molecular orbitals (RLMOs) based on a singular value decomposition algorithm, which should be faster than the localization methods described previously.[39,43] Then, we apply the LEA-TDDFT, LEA-TDHF, or LEA-CIS method to investigate the $n \rightarrow \pi^*$ electronic transition of acetone in aqueous solution. Previously, although a number of theoretical studies[6,44−56] have been reported for this system, the acetone−water clusters we adopt here are much larger than those used by others at the same level of theory. We anticipate that this work can provide more accurate descriptions (due to the use of large acetone−water clusters), leading to a better understanding of the solvent effect on the $n \rightarrow \pi^*$ electronic transition of acetone.

dx.doi.org/10.1021/ct500551p | J. Chem. Theory Comput. XXXX, XXX, XXX−XXX

2. METHODOLOGY

2.1. TDDFT and TDHF (or CIS) Equations Based on Localized Molecular Orbitals (LMO-TDDFT, LMO-TDHF, or LMO-CIS). In TDDFT theory, the working equation can be written as a non-Hermitian eigenvalue equation,[34−36]

$$\begin{bmatrix} A & B \\ B^* & A^* \end{bmatrix}\begin{bmatrix} X \\ Y \end{bmatrix} = \omega\begin{bmatrix} 1 & 0 \\ 0 & -1 \end{bmatrix}\begin{bmatrix} X \\ Y \end{bmatrix} \tag{1}$$

where the elements of the matrices A and B are defined as follows,

$$A_{ia,jb} = (\varepsilon_a - \varepsilon_i)\delta_{ij}\delta_{ab} + (ia|jb) - c_{HF}(ij|ab) + (1 - c_{HF})(ia|f_{xc}|jb) \tag{2}$$

$$B_{ia,jb} = (ia|bj) - c_{HF}(ib|aj) + (1 - c_{HF})\,(ia|f_{xc}|bj) \tag{3}$$

In the equations above, c_{HF} is the parameter of the Hartree−Fock exchange in the xc potential in a hybrid functional (c_{HF} is zero for a pure functional), the two-electron integrals are given in Mulliken notation, i, j, k, and l are used as the indices for occupied spin canonical molecular orbitals (CMOs), whereas a, b, c, and d are used as the indices for unoccupied spin CMOs, ε_a and ε_i are orbital energies of unoccupied and occupied CMOs, respectively. The term $(ia|f_{xc}|jb)$ is defined as[11]

$$(ia|f_{xc}|jb) = \int d\chi_1 d\chi_2 \varphi_i(\chi_1)\varphi_a(\chi_1)\frac{\delta^2 E_{xc}}{\delta\rho(r_1)\delta\rho(r_2)}\varphi_j(\chi_2)\varphi_b(\chi_2) \tag{4}$$

When $c_{HF} = 1$, the exchange-correlation term will disappear in eqs 2 and 3, and the working equations of TDHF are recovered.

The solution of eq 1 will yield the excitation energies ω and transition amplitudes. When the $\boldsymbol{B}$ matrix in the TDHF equation is set to zero, the TDHF equation becomes the CIS equation. This approximation is well-known as the Tamm−Dancoff approximation[57]

With localized molecular orbitals (LMOs), the Fock matrix F will not be diagonal, and then, the matrix elements of the A and B matrices in the LMO-TDDFT working equation are defined as below,

$$A^{LMO}_{ia,jb} = \delta_{ij}F^{LMO}_{ab} - \delta_{ab}F^{LMO}_{ij} + (ia|jb)^{LMO} - c_{HF}(ij|ab)^{LMO} + (1 - c_{HF})\,(ia|f_{xc}|jb)^{LMO} \tag{5}$$

$$B^{LMO}_{ia,jb} = (ia|bj)^{LMO} - c_{HF}(ib|aj)^{LMO} + (1 - c_{HF}) \times (ia|f_{xc}|bj)^{LMO} \tag{6}$$

It is worth mentioning that the transformation from CMOs to LMOs is a unitary transformation, which makes excitation energies invariant. Similarly, one can easily get the LMO-TDHF and LMO-CIS working equations.

2.2. Construction of the Regional Localized Molecular Orbitals. For a supermolecule (or cluster) containing a solute and many solvent molecules, we can partition it into two parts (active and environmental regions, denoted as $\boldsymbol{A}$- and $\boldsymbol{E}$-region, respectively). As shown in Figure 1, the $\boldsymbol{A}$-region may include the target solute and its neighboring six water molecules (denoted by a ball-and-stick model), while the $\boldsymbol{E}$-region contains all the remaining water molecules. Next, we will introduce an efficient localization scheme to get regional LMOs (RLMOs), which are localized on the active region. The basic idea is to find a unitary transformation that transforms the canonical occupied (or virtual) MOs of the supermolecule into RLMOs, which are mainly localized on the $\boldsymbol{A}$-region or $\boldsymbol{E}$-region. Mathematically, the subspace of occupied and virtual RLMOs in the $\boldsymbol{A}$-region (or $\boldsymbol{E}$-region) is required to have the maximum overlap with the orbital subspace of the supermolecule in the $\boldsymbol{A}$-region (or $\boldsymbol{E}$-region). One can use the following procedure to get RLMOs.

First, one should carry out DFT (or HF) calculations on the supermolecule and the active region (called as subsystem $\boldsymbol{A}$) to get the occupied (or virtual) canonical MOs $\{|\psi_i\rangle\}$ for the total system and the occupied (or virtual) canonical MOs $\{|\phi_j\rangle\}$ for the subsystem $\boldsymbol{A}$, respectively. Then, we can construct the overlap matrix between the canonical occupied MOs in the subsystem $\boldsymbol{A}$ and those in the whole system as an $N_o \times N_o^A$ matrix D^o (N_o^A and N_o are the number of the occupied orbitals in the subsystem $\boldsymbol{A}$ and the total system, $N_o > N_o^A$), as follows,

$$D^o_{ij} = \langle\psi_i|\phi_j\rangle \tag{7}$$

Assume that $\tilde{\psi}_i$ and $\tilde{\phi}_j$ represent the unitary transformations of occupied MOs for the whole system and for the subsystem $\boldsymbol{A}$, respectively,

$$\tilde{\psi}_i = \sum_{l=1}^{N_o}\psi_l V_{li}, \quad i = 1, \cdots, N_o \tag{8}$$

$$\tilde{\phi}_j = \sum_{k=1}^{N_o^A}\phi_k U_{kj}, \quad j = 1, \cdots, N_o^A \tag{9}$$

In the next step, our task is to require the overlap matrix between the transformed orbitals as described above to become an $N_o \times N_o^A$ diagonal matrix d^o by choosing an $N_o^A \times N_o^A$ unitary matrix U and an $N_o \times N_o$ unitary matrix V, that is,

$$d^o = V^\dagger D^o U \tag{10}$$

In reverse, the equation above can be rewritten as the formula below,

$$D^o = V d^o U^\dagger \tag{11}$$

Hence, this procedure is equivalent to perform a singular value decomposition (SVD) of the overlap matrix D^o. For each transformed occupied orbital $|\tilde{\phi}_j\rangle$ in the subsystem $\boldsymbol{A}$, there exists only a transformed occupied orbital $|\tilde{\psi}_i\rangle$ in the whole system so that the overlap d_j between them (a pair of the corresponding orbitals) is nonzero, as shown below,

$$\langle\tilde{\psi}_i|\tilde{\phi}_j\rangle = [V^\dagger D^o U]_{ij} = \delta_{ij}d_j \tag{12}$$

These transformed occupied orbitals of the whole system (whose number is just the number of occupied MOs in the subsystem $\boldsymbol{A}$) can be defined as occupied regional LMOs in the subsystem $\boldsymbol{A}$ (the remaining transformed occupied orbitals may be considered as regional LMOs of the $\boldsymbol{E}$-region). Similarly, one can apply a similar procedure as described above to obtain virtual regional LMOs in the subsystem $\boldsymbol{A}$. If the overlap integral d_j of a pair of the corresponding orbitals is close to unity, the RLMO is highly localized in the subsystem $\boldsymbol{A}$. For acetone−water clusters, our calculations show that the overlap integrals are always larger than 0.99 for occupied RLMOs (or 0.70 for virtual RLMOs) in the active region. This result suggests that the obtained occupied and virtual RLMOs are

dx.doi.org/10.1021/ct500551p | J. Chem. Theory Comput. XXXX, XXX, XXX−XXX

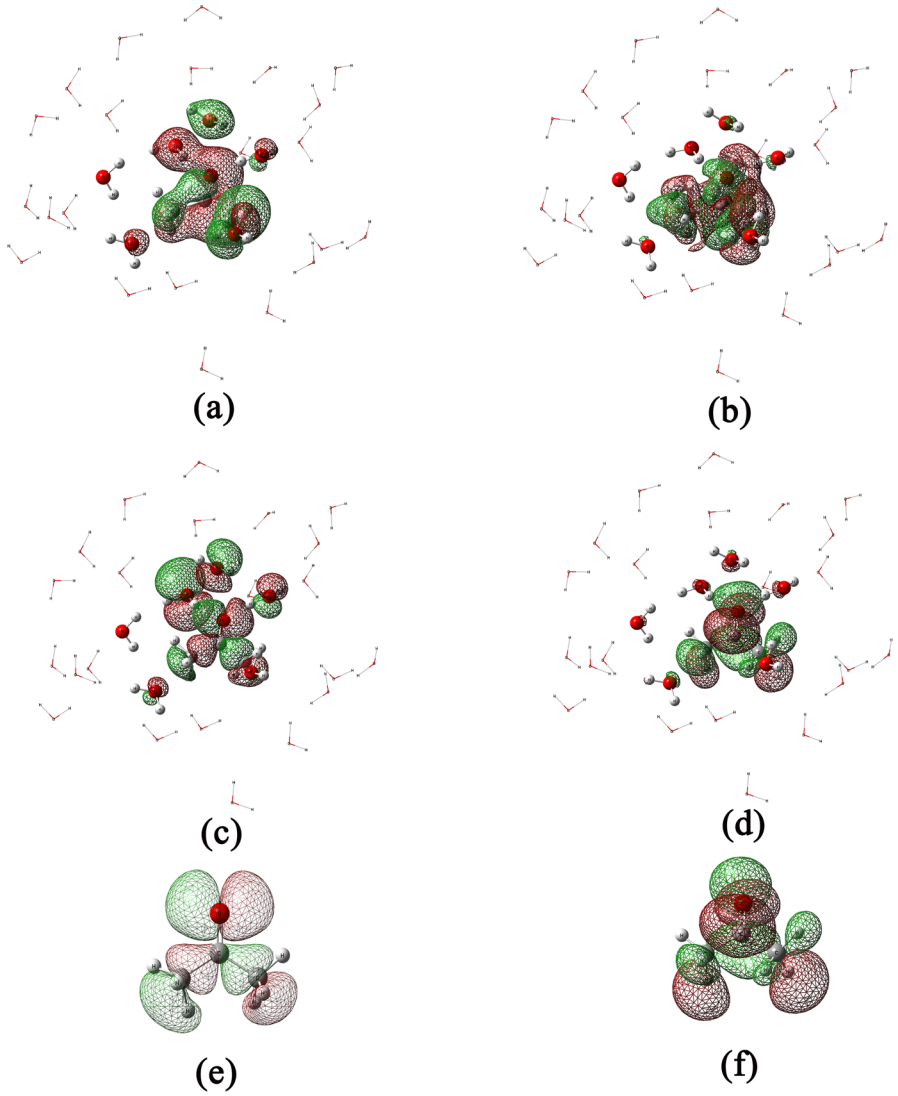

Figure 2. Schematic representation for (a) an occupied RLMO, and (b) an unoccupied RLMO; (c) an occupied QCMO (HOMO, *n*-like orbital), and (d) an unoccupied QCMO (LUMO, π^*-like orbital), in the active region of an acetone−water cluster; (e) an occupied CMO (HOMO, *n* orbital) and (f) an unoccupied CMO (LUMO, π^*orbital) of an acetone molecule.

quite local in the active region (a solute and a few neighboring solvents).

It should be pointed out that the localization scheme described above is similar to the Mayer's method[58] based on Löwdin's pairing theorem[59] for obtaining a subset of occupied localized orbitals in a given fragment of a large system. The difference is that the orthonormal basis sets in the fragment are replaced by the orthonormal DFT (or HF) orbitals from DFT (or HF) calculations on the subsystem ***A*** (which corresponds to a closed-shell subsystem for the studied system). In addition, both occupied and virtual LMOs localized in the subsystem ***A*** are obtained with the present scheme.

The procedure to get regional LMOs can be easily implemented. For example, two RLMOs in the active region ***A*** of the supermolecule (shown in Figure 1) obtained with the above procedure are displayed in Figure 2a and b. It can be seen that two RLMOs are well localized on the *A*-region.

2.3. Local Excitation Approximation. For certain excited state which shows strong local character, the TDDFT working equation of the total system can be reduced to the following form,

$$\begin{bmatrix} A_{\text{active}} & B_{\text{active}} \\ B^*_{\text{active}} & A^*_{\text{active}} \end{bmatrix} \begin{bmatrix} X_{\text{active}} \\ Y_{\text{active}} \end{bmatrix} = \omega \begin{bmatrix} I & 0 \\ 0 & -I \end{bmatrix} \begin{bmatrix} X_{\text{active}} \\ Y_{\text{active}} \end{bmatrix} \quad (13)$$

Here, the matrix A (or B) represents a small block of the original A (or B) matrix, in which all MO indices belong to the active region ***A*** (i.e., they are RLMOs). Equation 13 can be considered as the local excitation approximation (LEA) of the TDDFT working equation (LEA-TDDFT in short). Assume the occupied and virtual RLMOs in the active region are n_o and n_v, respectively. The dimension of matrix A (or B) in LAE-TDDFT is $n_o \times n_v$, while that in conventional TDDFT is $N_o \times N_v$ ($N_{o(v)}$ is the corresponding occupied (virtual) molecular orbital in the total system, usually $N_{o(v)} \gg n_{o(v)}$). Hence, the size of the LEA-TDDFT working matrix will be dramatically reduced if the selected active region is a small part of the total system.

It should be emphasized that the use of RLMOs may lead to the slow convergence of Davidson's iterative diagonalization scheme[37] in solving the LEA-TDDFT equations, due to the dense structure of the RLMO-based LEA-TDDFT matrix. As suggested by Miura et al.,[39] an effective way to avoid this

dx.doi.org/10.1021/ct500551p | J. Chem. Theory Comput. XXXX, XXX, XXX−XXX

problem is to transform the RLMOs in the active region into quasi-canonical molecular orbitals (QCMOs), which are generated by unitary transformations from the RLMOs in occupied and virtual spaces, respectively. The unitary transformation matrices can be obtained by diagonalizing the RLMO-based Fock matrix within the occupied and virtual subspaces, respectively. The number of occupied (or virtual) QCMOs is just the number of occupied (or virtual) RLMOs in the active region (denoted as n_o or n_v). With these QCMOs, the iterative diagonalization scheme of solving the LEA-TDDFT equation will converge must faster than that with RLMOs.

For example, two QCMOs (HOMO and LUMO) in the active region $\boldsymbol{A}$ of the supermolecule (shown in Figure 1) are shown in Figure 2c and d. These two QCMOs are very similar to the HOMO and LUMO of the separated acetone, displayed in Figure 2e and f, respectively.

The corresponding QCMO-based A and B matrix elements can be expressed as below,

$$A_{ia,jb}^{\mathrm{QCMO}} = \delta_{ij}\delta_{ab}(\lambda_a^{\mathrm{QCMO}} - \lambda_i^{\mathrm{QCMO}}) + (ia|jb)^{\mathrm{QCMO}} - c_{\mathrm{HF}}(ij|ab)^{\mathrm{QCMO}} + (1 - c_{\mathrm{HF}})\,(ia|f_{\mathrm{xc}}|jb)^{\mathrm{QCMO}} \tag{14}$$

$$B_{ia,jb}^{\mathrm{QCMO}} = (ia|bj)^{\mathrm{QCMO}} - c_{\mathrm{HF}}(ib|aj)^{\mathrm{QCMO}} + (1 - c_{\mathrm{HF}}) \times (ia|f_{\mathrm{xc}}|bj)^{\mathrm{QCMO}} \tag{15}$$

In this formula, $\lambda_a(\lambda_i)$ denotes the orbital energies of QCMOs.

2.4. Implementation of LEA-TDDFT. The implementation of LEA-TDDFT is very similar to that of the conventional TDDFT. The LEA-TDDFT programs include the following steps: (1) Perform a global SCF calculation for the target system to get occupied and virtual canonical molecular orbitals; (2) calculate the projected QCMOs (both occupied and virtual) in the active region. First, for the active region (which is a relatively smaller closed-shell cluster), we carry out an SCF calculation and then construct RLMOs in the active region. Then, we diagonalize the RLMO-based Fock matrix to obtain the QCMOs and their orbital energies. Next, we determine the projected QCMOs (both occupied and virtual), which are strictly localized on the active region. The reason why we need the projected QCMOs and how to get these projected QCMOs are described later in this subsection. (3) Solve the LEA-TDDFT eigenvalue equation with the projected QCMOs and their orbital energies. In studying the solvent effect, the target system is usually a large solute−solvent cluster, and its active region is selected as a small solute−solvent cluster, with one solute molecule surrounded by a few solvent molecules. When comparing the LEA-TDDFT method with the conventional TDDFT method, one can see that the first step is the same for both methods. The computational effort required in the second step is insignificant, compared to the third step (the solution of the LEA-TDDFT eigenvalue equation). In the third step, the dimension of the LEA-TDDFT eigenvalue equation is much less than that of the conventional TDDFT equation. Hence, the LEA-TDDFT calculation should be significantly faster than the conventional TDDFT calculation.

In general, we are only interested in obtaining the excitation energies of the LEA-TDDFT equations for a few low-lying excited states. These excitation energies can be determined by using the iterative diagonalization method.[37,60] In this technique, the original eigenvalue equations are solved in a small subspace of the trial vectors, in which the key quantities to be calculated are the sigma vectors. These sigma vectors can be obtained directly from the one- and two-electron integrals and the integrals can be computed on-the-fly as needed. The most expensive step in the calculation of the sigma vectors is to compute the following Fock-like matrix if a hybrid functional is used,[61]

$$\tilde{F}_{ia} = \sum_{\mu\nu} C_{\mu a}^{*}\tilde{F}_{\mu\nu}C_{\nu i} \tag{16}$$

where the Fock-like matrix over atomic orbitals ($\tilde{F}_{\mu\nu}$) and the density matrix-like matrix ($\tilde{P}$) are defined as

$$\tilde{F}_{\mu\nu} = \sum_{\lambda\sigma} (\mu\nu||\lambda\sigma)\tilde{P}_{\lambda\sigma} \tag{17}$$

$$\tilde{P}_{\lambda\sigma} = \sum_{jb} C_{\lambda j}^{*}c_j^b C_{\sigma b} \tag{18}$$

Here, C is the molecular orbital coefficient matrix and c_j^b represents the trial vectors. It can be seen that the computation of the Fock-like matrix ($\tilde{F}$) over atomic orbitals, which scales as the fourth power of the number of the basis functions (N), is the rate-determining step.

In solving the LEA-TDDFT eigenvalue equation, the computation of the Fock-like matrix will become a bottleneck for LEA-TDDFT calculations (although the iterative diagonalization step of LEA-TDDFT is much faster than that of the conventional TDDFT). Fortunately, the computation of the Fock-like matrix in LEA-TDDFT can be dramatically simplified if the local character of QCMOs in the active region can be exploited. Our strategy is to determine a projected molecular orbital $\bar{\Phi}_i$ within the active region for each QCMO Φ_i (which may have insignificant tails in the remaining region) and replace each QCMO with its projected QCMO in computing the Fock-like matrix. Assume that all atom-centered basis functions within the active region constitute an atomic orbital (AO) domain Ω, then each projected molecular orbital is expressed as follows:

$$|\bar{\Phi}_i\rangle = \sum_{\Omega} D_{si}|\chi_s\rangle \tag{19}$$

As suggested previously,[62,63] the expansion coefficients D_{si} can be determined by computing the functional,

$$\mathrm{W}(\bar{\Phi}_i) = \min \int (\Phi_i(r) - \bar{\Phi}_i(r))^2 \mathrm{d}r \tag{20}$$

Minimization of the functional $\mathrm{W}(\bar{\Phi}_i)$ leads to a set of linear equations for solving the expansion coefficients. Usually, $\bar{\Phi}_i$ is a very good approximation to $\bar{\Phi}_i$. With these projected QCMOs, we only need to calculate the Fock-like matrix with two-electron integrals over atomic orbitals within the active region. This step only scales as the fourth power of the number of the basis functions within the active region, which is much less than the number of basis functions in the whole system. Thus, with the tricks described above, we can apply the present LEA-TDDFT (TDHF, CIS) scheme to treat low-lying excited states, which are localized in a certain region, for very large systems.

2.5. Computational Details. The molecular dynamics (MD) simulations have been performed with the Tinker package[64−66] to generate acetone−water configurations. For acetone in aqueous solution, we consider a cubic box containing 519 water molecules and a single acetone molecule at the temperature of 298.15 K using the OPLSAA force field.[67,68] Periodic boundary conditions were used, and the time

dx.doi.org/10.1021/ct500551p | J. Chem. Theory Comput. XXXX, XXX, XXX−XXX

step was 1 fs. A spherical cutoff distance of 12.0 Å was used to truncate all nonbonded interactions. The equilibration time was set to be 600 ps, the production run was 600 ps (600 000 time steps), and configurations were dumped every 1000 time step (every 1 ps). Thus, a total of 600 configurations will be considered in the following TDDFT or TDHF (or CIS) calculations. The simulation was performed under the experiment liquid density for water ($\rho_{298.15}$ = 997.0470 kg/m^3),[69] which corresponds to a side length 25.0 Å of the cubic box. For acetone in gas-phase, we also performed the MD simulation under the similar conditions (except only a single acetone in the same cubic cell with a side of 25 Å). The starting structure is the optimized structure of acetone (as shown in Figure 3). The equilibration and sampling settings of simulation in gas phase are set to be the same as those in aqueous solution.

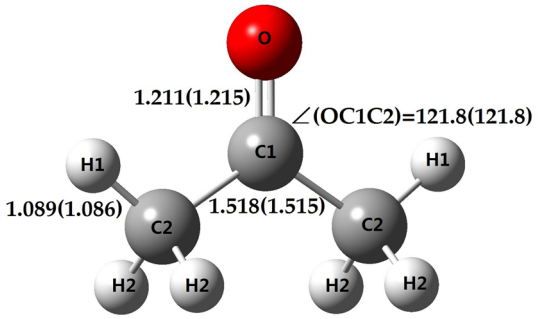

Figure 3. Optimized structure of acetone in vacuum obtained at the B3LYP/6-311++G(d) level (bond distances are in Ångstrom and bond angles are in degree). Experimental values (from ref 79) are included in parentheses for comparison.

In order to treat the solvent effect accurately, one should consider sufficiently large solute−solvent clusters. In this work, each cluster contains 519 water molecules and 1 acetone molecule. If the shortest distance from one water molecule to the oxygen atom of the solute molecule is smaller than 6.0 Å, the water molecule is treated as an explicit solvent, and other waters beyond this distance are considered as point charges in the total Hamiltonian. Usually, these "electrostatically embedded" clusters contain 25−42 water molecules and 1 acetone molecule. The point charges on all water molecules are obtained by performing generalized energy-based fragmentation (GEBF)[70,71] calculations for the original cluster (with 519 water molecules and 1 acetone molecule) at the HF/6-31G level. In the GEBF approach, the ground-state energy or properties (such as atomic charges, dipole moments, and so on) of a large system can be directly estimated with the corresponding quantities of small "electrostatically embedded" subsystems, which can be computed easily with existing quantum chemistry programs. To ensure the accuracy of the LEA scheme, we choose one acetone plus six nearest waters as the active region for each acetone−water cluster configuration. We describe the molecules in the active region using the 6-311++G(d) basis set[72,73] and use the 6-31G basis set[74] to describe the remaining molecules.

The molecular geometry optimization of acetone in gas phase has been performed by the Gaussian 09 package.[75] The conventional TDDFT, TDHF, and CIS calculations for various "electrostatically embedded" acetone−water clusters in this work were performed with the Gaussian 09 package and the GAMESS (US) program.[76] The LEA-TDDFT, LEA-TDHF, and LEA-CIS calculations were performed by the locally modified GAMESS program. The parameter-free hybrid PBE0[77] density functional is used in LEA-TDDFT computations, since it was demonstrated to provide satisfactory descriptions for the shift of $n \rightarrow \pi^*$ excitation of acetone in aqueous solution.[6,52]

In Table 1, we have listed the deviations of vertical $n \rightarrow \pi^*$ excitation energies calculated by LEA-TDDFT from TDDFT results of the full system for randomly selected 10 acetone−water clusters ("electrostatically embedded" clusters). As described in the preceding section, the HOMO and LUMO in an acetone−water cluster are very similar to those in the separated acetone, which correspond to *n*-like and π^*-like orbitals, respectively. The lowest excitation singlet state of acetone−water clusters may also be labeled as $n \rightarrow \pi^*$excitation (the coefficient of this excitation being about 0.9 for all clusters). The average deviation of LEA-TDDFT excitation energies from TDDFT results of the full system is 0.030 ± 0.006 eV. Similarly, at the TDHF level, we find that the average deviation of LEA-TDHF excitation energies from full system TDHF results is 0.022 ± 0.003 eV. Therefore, our calculations show that the LEA method has a good performance for the $n \rightarrow \pi^*$vertical electronic excitation of acetone in aqueous solution. While the average deviation of vertical $n \rightarrow \pi^*$ excitation

Table 1. Deviations of the Vertical Electronic $n \rightarrow \pi^*$ Excitation Energies (in eV) Calculated by LEA-TDDFT (ΔE_{LEA}) with Respect to the Full System TDDFT Results (ΔE_{full}) for 10 Randomly Selected Acetone−Water Clusters Generated in MD Simulations[a]

configuration	ΔE_{ref}	ΔE_{LEA}	ΔE_{full}	$\lvert\Delta E_{LEA} - \Delta E_{full}\rvert$	$\lvert\Delta E_{ref} - \Delta E_{full}\rvert$
1	4.275	4.336	4.303	0.033	0.028
2	4.297	4.397	4.367	0.030	0.070
3	4.366	4.411	4.389	0.022	0.023
4	4.387	4.583	4.554	0.029	0.167
5	4.646	4.704	4.668	0.036	0.022
6	4.310	4.391	4.368	0.023	0.058
7	4.448	4.625	4.592	0.033	0.144
8	3.941	4.108	4.078	0.030	0.137
9	4.235	4.344	4.321	0.023	0.086
10	4.446	4.542	4.503	0.039	0.057
avg.				0.030 ± 0.006	0.078 ± 0.053

[a]The results obtained for the active region (one acetone and six nearest-neighboring water molecules) alone, denoted by ΔE_{ref}, are also listed for comparison.

dx.doi.org/10.1021/ct500551p | J. Chem. Theory Comput. XXXX, XXX, XXX−XXX

Table 2. CPU Time (in Seconds) Needed by LEA-TDDFT for Obtaining the $n \rightarrow \pi^*$ Electronic Excitation Energy of Acetone in Aqueous Solution[a]

	present scheme				conventional scheme			
conf.	SCF	QCMO[a]	LEA-TDDFT[b]	total	SCF	TDDFT[b]	total	ratio[c]
1	2994	392 + 1 + 33	3572	6992	2994	45843	48837	7
2	2787	408 + 1 + 36	3878	7110	2787	55183	57970	8
3	2530	366 + 1 + 34	3279	6210	2530	49984	52514	8
4	2795	408 + 1 + 34	3919	7157	2795	49050	51845	7
5	2559	383 + 1 + 37	3241	6221	2559	43802	46361	7
6	2946	378 + 1 + 36	3436	6797	2946	48633	51579	8
7	3349	389 + 1 + 34	3323	7096	3349	67531	70880	10
8	2932	388 + 1 + 32	3306	6659	2932	41819	44751	7
9	2273	384 + 1 + 31	3216	5905	2273	35057	37330	6
10	3382	362 + 1 + 32	3356	7133	3382	64040	67422	10
avg.	2855	421	3453	6728	2855	50094	52949	8

[a]In the column, the first number denotes the time of SCF calculation on the active region, the second is the time required in transforming CMOs to RLMOs, the last one is the time needed in transforming RLMOs to QCMOs and calculating projected QCMOs. [b]The time needed for solving the LEA-TDDFT (or TDDFT) working equation. [c]The ratio means the times of the total time of TDDFT with respect to the total time of LEA-TDDFT. [a]The CPU time needed by conventional TDDFT are also listed for comparison.

energies calculated by TDDFT (TDHF) on the active region alone from TDDFT (TDHF) results of the full system is about 0.079 ± 0.053 eV (0.116 ± 0.060 eV). This result shows that the neighboring water molecules around the active region have a significant impact on the vertical $n \rightarrow \pi^*$ excitation energies. To understand the actual computational savings of LEA-TDDFT over the conventional TDDFT, we list in Table 2 various timings of different steps, which have been discussed in the preceding subsection, in LEA-TDDFT and TDDFT calculations on 10 randomly selected configurations. All calculations are performed on one Intel(R) Xeon E5-2670 2.60 GHz processor. One can see from Table 2 that the computational time of getting the projected QCMOs of the active region is much less than that of the solution of the LEA-TDDFT eigenvalue equation. The cost of solving the LEA-TDDFT equation is comparable to that of the global SCF calculation for the system under study. For even larger acetone−water clusters, the global SCF calculation may be more expensive than the solution of the LEA-TDDFT equation (if the active region is chosen to be the same). The time of solving the full system TDDFT equation is about 35 000−70 000 s, while that of solving the corresponding LEA-TDDFT equation is only about 3000−4000 s. This result is understandable, because the dimension of the working matrix A (or B) for the full system TDDFT calculation is about 80 000−120 000, while that of the corresponding matrix in the LEA-TDDFT scheme is only about 10 000. The computational speed of a complete LEA-TDDFT calculation (including the global SCF calculation) is about 6−10 times faster than that of the full system TDDFT calculation, dependent on the chosen acetone−water cluster. Usually, one can complete an LEA-TDDFT calculation for a large acetone−water cluster (1 acetone plus 25−42 water) within 2 h (with the computer described above). It could be expected that the present scheme will bring even more computational savings if larger acetone−water clusters are employed.

3. RESULTS AND DISCUSSIONS

In this section, we will first calculate the $n \rightarrow \pi^*$ electronic excitation energy of acetone in vacuum. Then, we will discuss the shift in the $n \rightarrow \pi^*$ electronic excitation energy for acetone in aqueous solution.

First, the optimized gas-phase geometry of acetone is obtained at the B3LYP[78]/6-311++G (d) level, as shown in Figure 3. One can see from Figure 3 that the optimized geometrical data are in good agreement with the available experimental data.[79] Table 3 shows the geometrical parameters

Table 3. Geometrical Parameters of the Acetone Molecule Averaged over 600 Configurations in MD Simulations, and the corresponding Gas-Phase Experimental Values from Ref 79[a]

	MD simulation		
	gas phase	aqueous solution	experimental gas phase
	Bond Distance (Å)		
C═O	1.229(0.022)	1.234(0.023)	1.215(0.005)
C—C	1.526(0.022)	1.522(0.020)	1.515(0.005)
C—H	1.091(0.011)	1.090(0.012)	1.086(0.010)
	Bond Angle (deg)		
C—C═O	121.0(2.8)	121.1(2.7)	122.0
C—C—C	117.8(2.9)	117.6(2.9)	116.1
C—C—H	110.0(4.7)	110.3(4.7)	110.3

[a]The values in parentheses represent the standard deviations.

for acetone, obtained with the statistical average over 600 configurations from gas-phase MD simulations. The average carbonyl bond length from the present classical MD is 1.229 ± 0.022 Å, in excellent agreement with the result (1.23 ± 0.02 Å) in a previous gas-phase Car−Parrinello molecular dynamics (CPMD) simulation.[6] With the 6-311++G(d) basis set, the average vertical $n \rightarrow \pi^*$ electronic excitation energy of acetone from 600 configurations is 4.248 ± 0.006 eV at the TDDFT (PBE0) level, 4.865 ± 0.006 eV at the TDHF level, or 5.027 ± 0.006 at the CIS level. The average TDDFT $n \rightarrow \pi^*$ excitation energy in gas phase is about 0.2 eV below the experimental data (4.488 eV),[80−82] while the TDHF and CIS methods provide less accurate results.

For acetone in aqueous solution, we first check the distribution of water molecules around acetone from MD simulations. The radial distribution functions (RDF) of O (acetone)−O (water) and O (acetone)−H (water) are displayed in Figure 4. A hydrogen bond peak starts around

dx.doi.org/10.1021/ct500551p | J. Chem. Theory Comput. XXXX, XXX, XXX−XXX

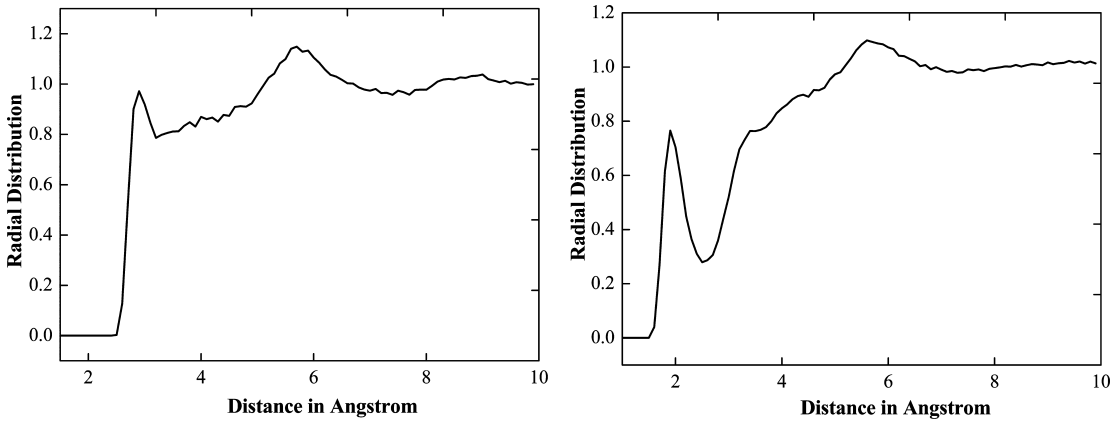

Figure 4. Radial distribution functions. (a) $O((CH_3)_2CO)-O(H_2O)$; (b) $O((CH_3)_2CO)-H$ (H_2O).

1.5 Å in the O−H RDF and around 2.5 Å in the O−O RDF, and ends at the O−H distance around 2.5 Å and O−O distance around 3.2 Å. The first maximums in the RDFs are at 1.9 Å (O−H) and 2.9 Å (O−O), respectively. Thus, a hydrogen bond length of about 1.9 Å is found, which indicates a strong hydrogen bond between acetone and a water molecule. From the fact that the H−O distance in water is 0.957 Å, one can conclude that the hydrogen bond is almost linear. Spherical integration of the first peak in the O−O RDF gives a coordination number of 1.9. Thus, we infer that the oxygen atom of acetone is involved in the formation of about two hydrogen bonds. These findings are similar to the results reported by Coutinho et al.[51] The results obtained above reveal that our treatment of including six water molecules into the active region is sufficiently accurate.

For acetone in aqueous solution, the average shift in the vertical $n \rightarrow \pi^*$ electronic excitation energy relative to that of acetone in gas phase calculated with the LEA-TDDFT, LEA-TDHF, and LEA-CIS schemes are shown in Table 4. The average shift is obtained as the statistical average over 600 acetone−water configurations generated in classical MD simulation. The selection criteria of these configurations and the computational details have been described in the previous subsection. In Table 3, we also list the average geometrical parameters for acetone (of acetone−water clusters), which are close to the gas-phase results.

Table 4. LEA-TDDFT, LEA-TDHF, and LEA-CIS Shifts (in cm^{-1}) in the $n \rightarrow \pi^*$ Electronic Excitation Energy of Acetone in Aqueous Solution Obtained with Different Number of Acetone−Water Configurations in the Statistical Averaging

configurations	LEA-TDDFT	LEA-TDHF	LEA-CIS
20	1670 ± 194	2549 ± 256	2734 ± 245
40	1645 ± 177	2806 ± 198	2638 ± 191
60	1565 ± 145	2738 ± 155	2573 ± 150
100	1460 ± 121	2615 ± 131	2452 ± 127
150	1547 ± 97	2733 ± 106	2565 ± 103
200	1581 ± 89	2729 ± 90	2565 ± 87
300	1581 ± 72	2746 ± 73	2581 ± 71
400	1613 ± 63	2790 ± 63	2621 ± 62
500	1621 ± 57	2790 ± 57	2621 ± 55
600	1621 ± 52	2790 ± 52	2613 ± 51

As seen from Table 4, the standard error of the average shift is gradually reduced when more configurations are included in the averaging procedure. In order to keep the standard error around 100 cm^{-1}, a minimum number of 150 configurations should be used. With 600 configurations, the standard error of the average shift is calculated to be around 50 cm^{-1} at the LEA-TDDFT, LEA-TDHF, and LEA-CIS levels. The calculated solvatochromic shift of the $n \rightarrow \pi^*$absorption transition is 1621 ± 52 cm^{-1} at the LEA-TDDFT (PBE0) level, being in good agreement with the experimental blue shift of 1500−1700 cm^{-1}.[80−82] The deviation of the LEA-TDHF (or -CIS) solvatochromic shift relative to the experimental value is significantly larger, being about 2800 and 2600 cm^{-1}, respectively. In Figure 5, we have shown the statistical distribution of the shifts in the $n \rightarrow \pi^*$ electronic excitation energy for 600 acetone−water configurations. One can see a widespread distribution in the values ranging from about −2500 cm^{-1} to about 6500 cm^{-1} at the three theory levels. Surprisingly, a small red shift occurs in some acetone−water configurations, although the statistical average leads to the blue shift.

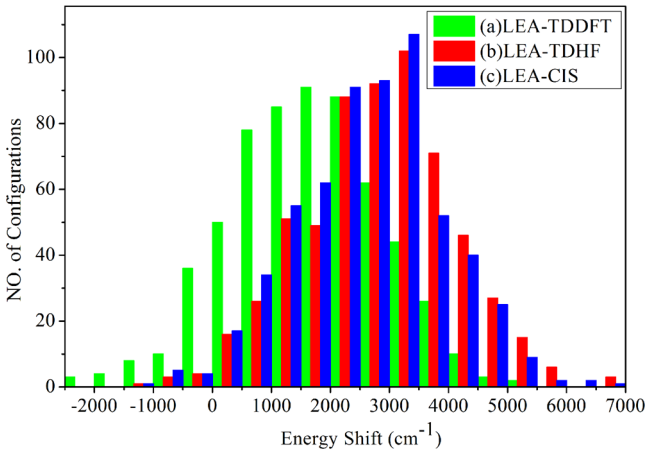

Figure 5. Statistical distributions of the shift in the $n \rightarrow \pi^*$ electronic excitation energy (relative to that in gas phase) for acetone in aqueous solution calculated with (a) the LEA-TDDFT scheme, (b) the LEA-TDHF scheme, and (c) the LEA-CIS scheme. Results are in cm^{-1}.

It should be mentioned that a variety of theoretical studies on the solvatochromic shift of the $n \rightarrow \pi^*$ excitation energy for acetone in solution have been reported.[6,44−56] For example,

dx.doi.org/10.1021/ct500551p | J. Chem. Theory Comput. XXXX, XXX, XXX−XXX

Gao[46] obtained a $n \rightarrow \pi^*$ blueshift of 1694 ± 84 cm^{-1} using the AM1-CI/molecular mechanics (MM) method (the solute treated by AM1-CI and the water molecules treated by MM) combined with MC simulations. Coutinho et al.[51] obtained 1150 ± 120 cm^{-1} using the CIS method and small acetone−water clusters (one solute plus two water molecules) from classical MC simulations. Coutinho et al.[45] also reported a blueshift of 1310 ± 40 cm^{-1} using the semiempirical INDO/CIS method and large acetone−water clusters (one solute plus 170 water molecules) from classical MC simulation. More sophisticated methods have also been used for the quantum description of the solute−solvent cluster. Aidas et al.[55] obtained a blueshift of 1103 ± 26 cm^{-1} using the EOM-CCSD/MM method (equation-of-motion coupled cluster singles and doubles, EOM-CCSD, for the solute and the polarized SPCpol force field for water molecules). Crescenzi et al.[6] also reported a blueshift of 1694 ± 81 cm^{-1} using the TD-DFT/PCM method and 100 acetone−water clusters (1 solute plus 3 water molecules) from CPMD simulation. In comparison with previous studies, this work differs mainly in that a large number of large acetone−water clusters (generated from classic MD simulations) are employed to study the solvatochromic shift at the LEA-TDDFT (TDHF and CIS) level of theory.

4. CONCLUSIONS

An efficient implementation of the local excitation approximation (LEA) of the TDDFT (TDHF, CIS) method has been developed in this work. The LEA-TDDFT (-TDHF, -CIS) method has been applied to investigate the solvatochromic shift of the $n \rightarrow \pi^*$ vertical excitation energy of acetone in aqueous solution. We have proposed an efficient localizing procedure to obtain regional localized molecular orbitals (RLMOs). To ensure the accuracy of the LEA scheme, we choose one acetone plus six nearest waters as the active region for each acetone−water cluster. Our illustrative applications demonstrated that the $n \rightarrow \pi^*$ excitation energies from the conventional TDDFT method with large acetone−water clusters could be well reproduced by the cost-effective LEA-TDDFT scheme based on a subset of RLMOs. Using the LEA scheme, we only need to perform TDDFT (TDHF or CIS) calculations on the active region (with a subset of RLMOs). The LEA-TDDFT calculations on 600 acetone−water configurations (from MD simulations) suggest that the blueshift in the $n \rightarrow \pi^*$ vertical electronic excitation energy for acetone in aqueous solution is 1621 ± 52 cm^{-1}, which is in good agreement with the available experimental blue shift of 1500−1700 cm^{-1}. The corresponding LEA-TDHF and LEA-CIS calculations tend to predict significantly larger blueshifts.

Although an efficient implementation of the LEA-TDDFT (-TDHF or -CIS) method is reported here, the LEA implementation of other excited state methods (such as SAC-CI[8], EOM-CC[9]) is straightforward. With various LEA-based excited state methods, one can study locally excited electronic states for very large systems. More applications are expected in the near future.

AUTHOR INFORMATION

Corresponding Author

*E-mail: shuhua@nju.edu.cn.

Notes

The authors declare no competing financial interest.

ACKNOWLEDGMENTS

This work was supported by the National Basic Research Program (Grant No. 2011CB808501) and the National Natural Science Foundation of China (Grant Nos. 21333004 and 21361140376). Part of the calculations was performed at the High Performance Computing Center of Nanjing University and the Shanghai Supercomputer Center (SSC, China).

REFERENCES

(1) Kirkwood, J. G. *J. Chem. Phys.* **1934**, *2*, 351−361.
(2) Onsager, L. *J. Am. Chem. Soc.* **1936**, *58*, 1486−1493.
(3) Warshel, A.; Levitt, M. *J. Mol. Biol.* **1976**, *103*, 227−249.
(4) Tomasi, J. *Theor. Chem. Acc.* **2004**, *112*, 184−203.
(5) Tomasi, J.; Mennucci, B.; Cammi, R. *Chem. Rev.* **2005**, *105*, 2999−3094.
(6) Crescenzi, O.; Pavone, M.; De Angelis, F.; Barone, V. *J. Phys. Chem. B* **2005**, *109*, 445−453.
(7) Rowe, D. J. *Rev. Mod. Phys.* **1968**, *40*, 153.
(8) Nakatsuji, H. *Chem. Phys. Lett.* **1979**, *67*, 334−342.
(9) Stanton, J. F.; Bartlett, R. J. *J. Chem. Phys.* **1993**, *98*, 7029−7039.
(10) Hicks, J. C.; Chandross, M. *Phys. Rev. B* **1999**, *59*, 9699−9702.
(11) Hirata, S.; Head-Gordon, M. *Chem. Phys. Lett.* **1999**, *302*, 375−382.
(12) Wiberg, K. B.; de Oliveira, A. E.; Trucks, G. *J. Phys. Chem. A* **2002**, *106*, 4192−4199.
(13) Nakao, Y.; Choe, Y. K.; Nakayama, K.; Hirao, K. *Mol. Phys.* **2002**, *100*, 729−745.
(14) Ukai, T.; Nakata, K.; Yamanaka, S.; Kubo, T.; Morita, Y.; Takada, T.; Yamaguchi, K. *Polyhedron* **2007**, *26*, 2313−2319.
(15) Robinson, D.; Mcdouall, J. *J. Chem. Theory Comput.* **2007**, *3*, 1306−1311.
(16) Lyakh, D. I.; Ivanov, V. V.; Adamowicz, L. *J. Chem. Phys.* **2008**, *128*, 74101.
(17) Fang, T.; Shen, J.; Li, S. *J. Chem. Phys.* **2008**, *129*, 234106.
(18) Mizukami, W.; Kurashige, Y.; Ehara, M.; Yanai, T.; Itoh, T. *J. Chem. Phys.* **2009**, *131*, 174313.
(19) Shen, J.; Li, S. *J. Chem. Phys.* **2009**, *131*, 174101.
(20) Slavicek, P.; Martinez, T. J. *J. Chem. Phys.* **2010**, *132*, 234102.
(21) Chaudhuri, R. K.; Freed, K. F.; Chattopadhyay, S.; Mahapatra, U. S. *J. Chem. Phys.* **2011**, *135*, 84118.
(22) Gonzalez, L.; Escudero, D.; Serrano-Andres, L. *ChemPhysChem* **2012**, *13*, 28−51.
(23) Liu, F.; Kurashige, Y.; Yanai, T.; Morokuma, K. *J. Chem. Theory Comput.* **2013**, *9*, 4462−4469.
(24) Barcza, G.; Gebhard, F.; Legeza, O. *Mol. Phys.* **2013**, *111*, 2506−2515.
(25) Tomasello, G.; Garavelli, M.; Orlandi, G. *Phys. Chem. Chem. Phys.* **2013**, *15*, 19763−19773.
(26) Nakatani, N.; Wouters, S.; Van Neck, D.; Chan, G. K. *J. Chem. Phys.* **2014**, *140*, 24108.
(27) Shuai, Z.; Peng, Q. *Phys. Rep.* **2014**, *537*, 123−156.
(28) Capdevila-Cortada, M.; Ribas-Arino, J.; Novoa, J. J. *J. Chem. Theory Comput.* **2014**, *10*, 650−658.
(29) Sous, J.; Goel, P.; Nooijen, M. *Mol. Phys.* **2014**, *112*, 616−638.
(30) Fliegl, H.; Sundholm, D. *Phys. Chem. Chem. Phys.* **2014**, *16*, 9859−9865.
(31) Foresman, J. B.; Headgordon, M.; Pople, J. A.; Frisch, M. J. *J. Phys. Chem.* **1992**, *96*, 135−149.
(32) Dirac, P. A. M. *Proc. Cambridge Philos. Soc.* **1930**, *26*, 376−385.
(33) Heinrichs, J. *Chem. Phys. Lett.* **1968**, *2*, 315−318.
(34) Gross, E. K. U.; Runge, E. *Phys. Rev. Lett.* **1984**, *52*, 997−1000.
(35) Kohn, W.; Gross, E. K. U. *Phys. Rev. Lett.* **1985**, *55*, 2850−2852.
(36) Gross, E. K. U.; Kohn, W. *Adv. Quantum Chem.* **1990**, *21*, 255−291.
(37) Davidson, E. R. *J. Comput. Phys.* **1975**, *17*, 87−94.
(38) Li, Q.; Li, Q.; Shuai, Z. *Synth. Met.* **2008**, *158*, 330−335.
(39) Miura, M.; Aoki, Y. *J. Comput. Chem.* **2009**, *30*, 2213−2230.

(40) Imamura, A.; Aoki, Y.; Maekawa, K. *J. Chem. Phys.* **1991**, *95*, 5419−5431.
(41) Kurihara, Y.; Aoki, Y.; Imamura, A. *J. Chem. Phys.* **1997**, *107*, 3569−3575.
(42) Kurihara, Y.; Aoki, Y.; Imamura, A. *J. Chem. Phys.* **1998**, *108*, 10303−10308.
(43) Gu, F. L.; Aoki, Y.; Korchowiec, J.; Imamura, A.; Kirtman, B. *J. Chem. Phys.* **2004**, *121*, 10385−10391.
(44) Canuto, S.; Coutinho, K. *Int. J. Quantum Chem.* **2000**, *77*, 192−198.
(45) Coutinho, K.; Canuto, S. *J. Mol. Struct.: THEOCHEM* **2003**, *632*, 235−246.
(46) Gao, J. L. *J. Am. Chem. Soc.* **1994**, *116*, 9324−9328.
(47) Ten No, S.; Hirata, F.; Kato, S. *J. Chem. Phys.* **1994**, *100*, 7443−7453.
(48) Liao, D. W.; Mebel, A. M.; Chen, Y. T.; Lin, S. H. *J. Phys. Chem. A* **1997**, *101*, 9925−9934.
(49) Serranoandres, L.; Fulscher, M. P.; Karlstrom, G. *Int. J. Quantum Chem.* **1997**, *65*, 167−181.
(50) Grozema, F. C.; van Duijnen, P. T. *J. Phys. Chem. A* **1998**, *102*, 7984−7989.
(51) Coutinho, K.; Saavedra, N.; Canuto, S. *J. Mol. Struct.: THEOCHEM* **1999**, *466*, 69−75.
(52) Aquilante, F.; Cossi, M.; Crescenzi, O.; Scalmani, G.; Barone, V. *Mol. Phys.* **2003**, *101*, 1945−1953.
(53) Bernasconi, L.; Sprik, M.; Hutter, J. *J. Chem. Phys.* **2003**, *119*, 12417−12431.
(54) Rohrig, U. F.; Frank, I.; Hutter, J.; Laio, A.; Vandevondele, J.; Rothlisberger, U. *ChemPhysChem* **2003**, *4*, 1177−1182.
(55) Aidas, K.; Kongsted, J.; Osted, A.; Mikkelsen, K. V.; Christiansen, O. *J. Phys. Chem. A* **2005**, *109*, 8001−8010.
(56) Sulpizi, M.; Rohrig, U. F.; Hutter, J.; Rothlisberger, U. *Int. J. Quantum Chem.* **2005**, *101*, 671−682.
(57) Hirata, S.; Head-Gordon, M. *Chem. Phys. Lett.* **1999**, *314*, 291−299.
(58) Zoboki, T.; Mayer, I. *J. Comput. Chem.* **2011**, *32*, 689−695.
(59) Löwdin, P. *J. Appl. Phys.* **1962**, *33*, 251−280.
(60) Davidson, E. R. *J. Comput. Phys.* **1975**, *17*, 87−94.
(61) Maurice, D.; Head-Gordon, M. *J. Phys. Chem.* **1996**, *100*, 6131−6137.
(62) Boughton, J. W.; Pulay, P. *J. Comput. Chem.* **1993**, *14*, 736−740.
(63) Li, S.; Shen, J.; Li, W.; Jiang, Y. *J. Chem. Phys.* **2006**, *125*, 74109.
(64) Ponder, J. W.; Richards, F. M. *J. Comput. Chem.* **1987**, *8*, 1016−1024.
(65) Ren, P. Y.; Ponder, J. W. *J. Comput. Chem.* **2002**, *23*, 1497−1506.
(66) Ren, P. Y.; Ponder, J. W. *J. Phys. Chem. B* **2003**, *107*, 5933−5947.
(67) Jorgensen, W. L.; Maxwell, D. S.; Tiradorives, J. *J. Am. Chem. Soc.* **1996**, *118*, 11225−11236.
(68) Kaminski, G. A.; Friesner, R. A.; Tirado-Rives, J.; Jorgensen, W. L. *J. Phys. Chem. B* **2001**, *105*, 6474−6487.
(69) Tanaka, M.; Girard, G.; Davis, R.; Peuto, A.; Bignell, N. *Metrologia* **2001**, *38*, 301.
(70) Li, W.; Li, S.; Jiang, Y. *J. Phys. Chem. A* **2007**, *111*, 2193−2199.
(71) Li, S.; Li, W.; Ma, J. *Acc. Chem. Res.* **2014**, *47*, 2712−2720.
(72) Hehre, W. J.; Ditchfield, R.; Pople, J. A. *J. Chem. Phys.* **1972**, *56*, 2257−2261.
(73) Dill, J. D.; Pople, J. A. *J. Chem. Phys.* **1975**, *62*, 2921−2923.
(74) Francl, M. M.; Pietro, W. J.; Hehre, W. J.; Binkley, J. S.; Gordon, M. S.; Defrees, D. J.; Pople, J. A. *J. Chem. Phys.* **1982**, *77*, 3654−3665.
(75) Frisch, M. J.; Trucks, G. W.; Schlegel, H. B.; Scuseria, G. E.; Robb, M. A.; Cheeseman, J. R.; Montgomery, J. A. Jr.; Vreven, T.; Kudin, K. N.; Burant, J. C.; Millam, J. M.; Iyengar, S. S.; Tomasi, J.; Barone, V.; Mennucci, B.; Cossi, M.; Scalmani, G.; Rega, N.; Petersson, G. A.; Nakatsuji, H.; Hada, M.; Ehara, M.; Toyota, K.; Fukuda, R.; Hasegawa, J.; Ishida, M.; Nakajima, T.; Honda, Y.; Kitao, O.; Nakai, H.; Klene, M.; Li, X.; Knox, J. E.; Hratchian, H. P.; Cross, J. B.; Bakken, V.; Adamo, C.; Jaramillo, J.; Gomperts, R.; Stratmann, R. E.; Yazyev, O.; Austin, A. J.; Cammi, R.; Pomelli, C.; Ochterski, J. W.; Ayala, P. Y.; Morokuma, K.; Voth, G. A.; Salvador, P.; Dannenberg, J. J.; Zakrzewski, V. G.; Dapprich, S.; Daniels, A. D.; Strain, M. C.; Farkas, O.; Malick, D. K.; Rabuck, A. D.; Raghavachari, K.; Foresman, J. B.; Ortiz, J. V.; Cui, Q.; Baboul, A. G.; Clifford, S.; Cioslowski, J.; Stefanov, B. B.; Liu, G.; Liashenko, A.; Piskorz, P.; Komaromi, I.; Martin, R. L.; Fox, D. J.; Keith, T.; Al-Laham, M. A.; Peng, C. Y.; Nanayakkara, A.; Challacombe, M.; Gill, P. M. W.; Johnson, B.; Chen, W.; Wong, M. W.; Gonzalez, C.; Pople, J. A. *Gaussian 09*, Revision A.01; Gaussian, Inc.; Wallingford, CT, 2009.
(76) Schmidt, M. W.; Baldridge, K. K.; Boatz, J. A.; Elbert, S. T.; Gordon, M. S.; Jensen, J. H.; Koseki, S.; Matsunaga, N.; Nguyen, K. A.; Su, S. J.; Windus, T. L.; Dupuis, M.; Montgomery, J. A. *J. Comput. Chem.* **1993**, *14*, 1347−1363.
(77) Ernzerhof, M.; Scuseria, G. E. *J. Chem. Phys.* **1999**, *110*, 5029−5036.
(78) Becke, A. D. *J. Chem. Phys.* **1993**, *98*, 5648−5652.
(79) Swalen, J. D.; Costain, C. C. *J. Chem. Phys.* **1959**, *31*, 1562−1574.
(80) Bayliss, N. S.; Mcrae, E. G. *J. Phys. Chem.* **1954**, *58*, 1006−1011.
(81) Hayes, W. P.; Timmons, C. J. *Spectrochim. Acta* **1965**, *21*, 529−541.
(82) Bayliss, N. S.; Wills-Johnson, G. *Spectrochim. Acta, Part A* **1968**, *24*, 551−561.